Supplementary Materials for

Radio-Wave Heating of Iron Oxide Nanoparticles Can Regulate Plasma Glucose in Mice

Sarah A. Stanley, Jennifer E. Gagner, Shadi Damanpour, Mitsukuni Yoshida, Jonathan S. Dordick, Jeffrey M. Friedman*

*To whom correspondence should be addressed. E-mail: friedj@mail.rockefeller.edu

Published 4 May 2012, *Science* **336**, 604 (2012)
DOI: 10.1126/science.1216753

This PDF file includes:

SUPPORTING ONLINE MATERIAL

Materials and Methods

Nanoparticles

Iron oxide nanoparticles (10-50 nm diameter), functionalized with a surface carboxylic acid group, were purchased from Ocean Nanotech (Springdale, Arkansas). The nanoparticles were conjugated to either mouse monoclonal anti-His antibody (AbD Serotec, Raleigh, NC) or streptavidin (Jackson Immunoresearch Laboratories, West Grove, PA) using carbodiimide and N-hydroxysuccinimide activation technique as employed by magnetic nanocrystal conjugation kit (Ocean Nanotech). Heating studies were performed using 1 ml of a bulk solution (1 mg/ml) of nanoparticles dispersed in water placed in an eppendorf inside the solenoid and the temperature of the suspension was monitored using a fiber optic system (Luxtron, Lambda photometrics, Herts, UK).

RF magnetic-field

A 465 kHz sinusoidal signal was provided by a signal generator and applied through an amplifier (both Ultraflex, Ronkonkoma, NY) to a 2-turn solenoid coil with a radius of 2.5 cm to produce a magnetic field strength of 5 mT. Samples were placed within the solenoid. A 13.56 Mhz sinusoidal signal was provided by a signal generator (RF Instrumentation, PA) and applied through an amplifier (Comdel, Gloucester, MA) to a 2-turn solenoid coil with a radius of 2.5 cm).

Plasmids

TRPV1 (in pcDNA3.1) was a kind gift of Wolfgang Liedkte (Duke University, NC) and cloned into pEGFP-N1 (Clontech, Mountainview, CA). It was modified by PCR (Fast start PCR, Roche) to introduce Hisx6. Nuclear factor of activated t-cells (NFAT) response elements and minimal promoter were from pGL4.30[*luc2P*/NFAT-RE/Hygro (Promega, Madison, WI). Serum response element (SRE), cyclic AMP response element (CRE) and furin modified human insulin sequences were synthesized by Integrated DNA technologies (Coralville, IO). The calcium dependent response elements – SRE, CRE and NFAT response elements were each used in triplicate. The use of these three response elements increased the likelihood that at least one such mechanism would be active with high sensitivity in all of the cell types that we engineered. They were also used to achieve high specificity since each of these elements is reported to respond only to repeated or sustained changes in intracellular calcium. BAPTM, the transmembrane domain of platelet derived growth factor receptor fused to an extracellular biotin acceptor protein, was a kind gift of Dr. B Tannous, Massachusetts General Hospital, MA). $TRPV1^{His}$ and calcium responsive furin insulin were cloned into MSCV-hygro and MSCV-puro plasmids (Clontech,) respectively for retrovirus production using Phoenix packaging cells. Mouse ferritin heavy chain was obtained from ATTC (Manassas, VA) in pCMV sport6 and mouse ferritin light chain 1 was obtained from Invitrogen (Carlsbad, CA) in pYX-Asc. These were cloned downstream of EF1alpha promoter in pCR2.1 with a flexible linker region to create ferritin light chain – linker – heavy chain fusion protein. The fidelity of PCR products was confirmed by DNA sequencing.

Cell culture and *in vitro* studies

Human embryonic kidney cells (HEK 293T) were cultured in Dulbecco's modified eagle medium with 10% fetal bovine serum (Gibco, Carlsbad, CA) at 37^{o}C and 5% CO_2. PC12 cells were cultured in RPMI medium 1640 with 10% horse serum and 5% fetal bovine serum (Gibco) at 37^{o}C and 5% CO_2. Phoenix ecotropic packaging cells (Stanford University) were grown in Dulbecco's modified eagle medium with 10% fetal bovine serum (Gibco) at 37^{o}C and 5% CO_2.

Stable cell lines were produced by retroviral infection of PC12 cells using the Phoenix system. Briefly, Phoenix eco cells (2 x 10^6 cells per 6-cm dish) were transfected with MSCV-puro or hygro plasmids as described above. After 24 hours, the medium was replaced and the cells placed at 32^{o}C. Medium was aspirated after a further 24 h and spun to remove cell debris. The Phoenix cell supernatant was added to PC12 cells (plated at 1 x 10^6 cells per 6-cm dish) using a 1:2 dilution in RPMI medium/10% FBS with polybrene (4 µg/ml, Sigma-Aldrich, St Louis, MO). Cells were incubated at 32^{o}C for a further 24 h before replacing the medium with RPMI/10% FBS. Selection medium was added 48 h after infection.

Embryonic stem cells were electroporated with a calcium dependent human insulin plasmid and selected with puromycin for 3 weeks. Resistant cells were identified for insulin insertion by Southern blot analysis before electroporation with TRPV1His plasmid and selection with hygromycin for 3 weeks. Three double resistant clones were screen by quantitative PCR for expression of insulin and TRPV1 and by immunohistochemistry for expression of TRPV1 and His tag. The ES clone with high expression by qPCR and IHC was used for RF studies. Cells were plated onto gelatin coated 12mm cover glass (without feeder cells) for 96 hrs before assessing RF dependent release of calcium dependent human insulin.

For immunocytochemistry and RF studies, cells were cultured on 12-mm cover glass (Fisher Scientific, Pittsburgh, PA) coated with collagen (BD biosciences, Bedford, MA) and poly-D-lysine (Millipore, Billerica, MA). For EM studies, cells were cultured in 3cm dishes. Cells were transfected 24 h after plating using lipofectamine 2000 (Invitrogen, Carlsbad, CA). For temperature dependent studies, cells were plated in 24-well plates coated with collagen and poly-D-lysine and transfected 24 h later. Culture medium was replaced 18 h after transfection and holotransferrin (2 mg/ml, Sigma) was added to cells transfected with ferritin. Cells were studied 72 h after transfection.

Temperature dependent release of calcium dependent human insulin: 24 h prior to the study, cells were placed in serum free medium at 32^{o}C to ensure minimal activation of TRPV1 and calcium dependent pathways. On the day of study, cells were preincubated for 30 min in 500 µl phosphate buffered saline (PBS) before incubation in 250 µl of calcium imaging buffer (*28*) at 32 or 44^{o}C for 1 h. At the end of 1 h, the supernatant was aspirated, spun to remove cell debris and frozen at -80^{o}C until assay. Studies were performed in quadruplicate on three occasions.

RF dependent release of calcium dependent human insulin: 24 h prior to the study, cells were placed in serum free medium at 32^{o}C to ensure minimal activation of TRPV1 and calcium dependent pathways. On the day of study, cells were preincubated for 30 min in 500µl PBS or 500 µl of functionalized iron oxide nanoparticles (1 mg/ml) resuspended in PBS. Cells were washed three times in PBS before incubation in 300 µl of calcium imaging buffer at room temperature (control) or in a RF field at room temperature. The supernatant was removed at 15, 30, 45 or 60 min depending on the study, spun to remove cell debris and frozen at -80^{o}C until assay. For gene expression analysis, cells from the supernatant and cover glass were lysed and the lysate stored at 80^{o}C until RNA purification. For apoptosis studies, the cells were incubated with functionalized nanoparticles at 1, 2, 4 or 8 mg/ml before RF treatment and immunocytochemistry. For RF dependent time course from stable PC12 cells, cells were left in serum containing medium prior to treatment to more accurately replicate conditions *in vivo* before performing the studies as described above. Medium was removed for assay at 15 and 30 mins.

For studies examining the role of TRP channels in RF mediated proinsulin release, ruthenium red (100µM) was added to the calcium imaging buffer. For studies to examine the role of calcineurin in the activation of calcium dependent insulin gene, Tacrolimus (100nM, Tocris Bioscience, Minneapolis, MN) was added to the medium for 24 hours prior to RF treatment. To examine if the effects of RF heating on iron oxide nanoparticles were confined to decorated cells, 3-cm dishes of HEK 293T cells were transfected with either BAPTM or TRPV1 and calcium dependent human insulin. After 24 h, the two transfected cell populations were trypsinized and mixed to form a co-culture with adjacent cells expressing BAPTM and TRPV1/human insulin.

Calcium Imaging

Transfected cells were washed three times in PBS then loaded with Fluo-4 3µM (Invitrogen) in the presence of sulfinpyrazone 500 µM (Sigma) for 60 min at room temperature. Cells were washed again in PBS then incubated for 30 min either with functionalized nanoparticles with sulfinpyrazone or in sulfinpyrazone in PBS. Cells were washed and then imaged in calcium imaging buffer. Imaging was performed using a Deltavision personal DV imaging system (Applied Precision, Issawaq, WA) equipped with a custom-made ceramic lens. Cells were imaged before and during RF treatment or before and after treatment with 200 µM 2 aminoethoxydiphenyl borate (2-APB).

Immunocytochemistry, Immunohistochemistry and Electron Microscopy

Immunocytochemistry (ICC) was used to detect and quantify apoptotic cells following RF field treatment. Two assays were employed, TUNEL assay visualized using Apoptag Fluorescein direct in situ apoptosis detection kit (Millipore) and ICC for activated caspase-3 (Promega). After RF treatment, cells were washed twice in PBS and then fixed for 15 min in 2% paraformaldehyde (Electron Microscopy Services, Hatfield, PA). Cells were then stained according to the manufacturers' protocols. Expression of NFAT1 was also examined using ICC. Control or RF treated transfected cells were washed and fixed as above then incubated in for 1 h in blocking buffer (3% BSA (Sigma) and 2% goat serum (Sigma) in PBS with 0.1% Triton-X (Sigma)). Following blocking cells were incubated

in primary antibody, rabbit anti-NFAT1 (Cell signaling), 1:50, diluted in blocking buffer overnight at 4 degrees. Cells were then washed three times in PBS before incubation in secondary antibody (goat anti-rabbit 488 1: 1000) diluted in blocking buffer for 1 h. The cells were then washed a further three times in PBS before inverting and mounting using Fluoromount with DAPI (Southern Biotech, Birmingham, AL).

ICC was also used to examine expression of ferritin fusion. Cells were washed twice with PBS, fixed and blocked as above. Cells were incubated in primary antibody, rabbit anti-ferritin light chain (Dako, Carpinteria, CA), 1:1000, diluted in blocking buffer for 1 h. Cells were washed three times in PBS before incubation in secondary antibody (goat anti-rabbit 488 1: 1000) diluted in blocking buffer for 1 h. The cells were washed a further three times in PBS before inverting and mounting using Fluoromount (Southern Biotech, Birmingham, AL).

Immunohistochemistry (IHC) was used to confirm expression of TRPV1 and His and quantify apoptotic cells in tumors. Tumors were fixed in 10% formalin (Sigma) at 4^{o}C overnight then placed in 30% sucrose in PBS at 4^{o}C for a further 24 h. Tissue was embedded in OCT and frozen before 20μm cryosections were cut and placed directly on glass slides. Slides were placed at 55 degrees for 1 h then stored at -80 ^{o}C before staining. Apoptag Fluorescein direct *in situ* apoptosis detection and IHC for activated caspase-3 were performed according to the manufacturers' instructions. Staining for TRPV1 and His was performed as follows. Slides were washed three times with PBS then incubated in blocking buffer for 2 h followed by overnight incubation at 4^{o}C with primary antibody diluted in blocking buffer (rabbit anti-TRPV1 1:500, mouse anti-His 1:1000 (Sigma)). Slides were washed 3-times in PBS and then incubated overnight at 4^{o}C with secondary antibody diluted in blocking buffer (goat anti-rabbit 488 and goat anti-mouse 594 both at 1:1000). Slides were washed 3-times in PBS before applying Fluoromount and a coverglass (Fisher Scientific).

Images were acquired using a Zeiss Axioplane microscope and captured digitally with separate band-pass filters using the multichannel module of the AxioVision Zeiss software. Additional images were acquired using confocal microscopy (LSM 510 laser scanning confocal microscope; Carl Zeiss MicroImaging, Inc.). Quantification of TUNEL and active caspase-3 immunostaining was performed by an investigator blinded to the treatment group.

Electron microscopy was used to quantify nanoparticle binding to the cell membrane and to image ferritin in transfected cells. Cells were fixed in 2% paraformaldehyde/2.5% glutaraldehyde/0.1M cacodylate buffer, pH 7.4, for 15 minutes before pelleting and further fixation for 1 h. Cells were then treated with 1% osmium tetroxide (1 h, on ice) and 0.5% uranyl acetate (1 h) before dehydration with graded ethanol and treatment with propylene oxide (2 x 15 min). The cells were infiltrated with 50% EPON epoxy resin (Miller-Stephenson, Sylmar, CA) and 50% propylene oxide overnight then 100% EPON (2 x 2 h) before curing at 60^{o}C for 2 days. Blocks were cut with a diamond knife on a Leica UltracutE (Buffalo Grove, IL) and ultra-thin (~70nm) sections were collected on uncoated 200mesh grids and stained with uranium and lead. Grids were viewed with a Tecnai SpiritBT Transmission Electron Microscope (FEI, Hillsboro, Oregon) at 80 KV and pictures were taken with Gatan 895 ULTRASCAN Digital Camera (Pleasanton, CA).

ImmunoEM was used to confirm binding of nanoparticles to TRPV1. HEK 293T cells were seeded on Aclar (Ted Pella Inc, Redding, CA) in 24 well plates and transfected with TRPV1His 24 hours later. 72 hours after transfection, cells were washed twice with PBS and incubated with anti-His coated iron oxide nanoparticles for 30 mins. Following two further PBS washes, cells were fixed in a fixative containing fresh 4.0% paraformaldehyde and 0.1 M sodium cacodylate buffer (pH 7.4) for overnight. Cells were processed for immunoelectron microscopy: after incubating with a blocking solution containing 3% BSA and 0.05% saponin in sodium cacodylate buffer for 20 min, the primary antibody was applied and incubated for overnight at 4°C; in the following day, after extensive wash secondary antibody conjugated with nanogold (Nanoprobes, Inc. Yaphank, NY) (1:50) was applied and incubated for 2 hours; subsequently, with series of wash, silver enhancement was conducted by using silver enhancement kit (Nanoprobes, Inc. Yaphank, NY). Cells were re-fixed with 2.5% glutaraldehyde in the cacodylate buffer, lightly postfixed with 1% osmium tetra-oxide (10 min), dehydrated by a graded series of ethanol, infiltrated with EMBed812 resin and embedded in the same resin. Ultra-thin sections were cut and examined in the electron microscope (100CX JEOL, Tokyo, Japan) with the digital imaging system (XR41-C, Advantage Microscopy Technology Corp, Danver, MA). Control experiment was done by following the same procedure except for the step of omitting primary antibody and applying the blocking solution, instead.

Animals and *In vivo* studies

Male athymic NCr-nu/nu mice (NCI-Frederick, 6 weeks old), an outbred strain, were used and housed under controlled light conditions (12 h light/12 h dark) and temperature (22°C), single-caged, and fed ad libitum on standard mouse chow. Animal care and experimental procedures were performed with the approval of the Animal Care and Use Committee of Rockefeller University (protocol 11421) under established guidelines.

To generate subcutaneous tumors, 5×10^6 PC12 cells stably expressing $TRPV1^{His}$ and calcium dependent human insulin or calcium dependent human insulin alone were re-suspended in a 1:1 mixture of PBS and growth-factor reduced Matrigel (BD biosciences) and injected into the flank of anesthetized mice bilaterally. Radiofrequency studies were performed 4 weeks later. Blood glucose was monitored weekly. Mice were fasted overnight before all studies.

Study 1: Mice with $TRPV1^{His}$/insulin xenografts (n = 7) were anesthetized with inhaled isoflurane. PBS or iron oxide nanoparticles functionalized with anti-His antibody were injected into the tumor (5 x 10 µl). After 30 min, mice were treated with an RF magnetic field for 30 min by placing in a solenoid connected to the RF generator. Tail vein samples were taken at -30 and 0 min before RF magnetic field treatment and at 10, 20, 30, 45, 60, 90 and 120 min after the onset of RF treatment. Retro-orbital blood was taken using EDTA coated capillary tubes at -30 and 30 min for plasma insulin measurement. As the mice are outbred and had high inter-individual variability in blood glucose, the studies were performed with a cross-over design with each mouse receiving first PBS and then one week later receiving nanoparticle injections. Nanoparticle injections could not be performed first because the particles remain within the tissue for prolonged periods (*29*).

Study 2: Mice with $TRPV1^{His}$/insulin xenografts (n = 6/group) were anesthetized and were randomized to receive either functionalized iron oxide nanoparticles or PBS. An identical treatment protocol to study 1 was used and intratumoral temperature and core body temperature were monitored using a fiber optic temperature monitoring system. Thermal imaging using FLIR infrared camera SC325 (North Billerica, MA) was performed on a subset of mice. After 120 min, the mice were sacrificed and the tumors removed. Each tumor was divided in two and one half snap frozen in liquid nitrogen for RNA extraction and the one half placed in 10% formalin for immunohistochemistry.

Study 3: Mice injected with PC12 cells stably expressing calcium dependent human insulin (n = 8) were used and study 1 repeated.

Study 4: Mice injected with PC12 cells expressing calcium dependent human insulin were used (n = 6/group) and study 2 repeated.

Study 5: Mice injected with PC12 cells expressing $TRPV1^{His}$ and calcium dependent human insulin were used (n=6/group) and study 1 was repeated using nanoparticles which had not been conjugated to anti-His antibody.

Study 6: Mice injected with PC12 cells expressing $TRPV1^{His}$ and calcium dependent human insulin were used (n=7/group). Study 1 was repeated with mice injected initially with PBS and treated with RF. Blood glucose and insulin were measured as described above. One week later, mice were injected with anti-His conjugated nanoparticles and treated with RF. Blood glucose was monitored as above. After a further week, mice received a second injection of anti-His conjugated nanoparticles, were treated with RF and blood glucose and insulin were measured.

Assays

Proinsulin was measured in cell supernatants by ELISA (Alpco, Salem, NH) according to manufacturer's protocol. Blood glucose was determined using a Breeze 2 glucometer (Bayer; Leverkusen, Germany). Blood was spun for 10 min and plasma was collected. Plasma levels of human insulin, produced by xenografts, were determined in mouse plasma by human specific ELISA (Alpco).

Real-Time PCR

Total RNA was isolated by homogenizing tissue in TRIzol reagent (Invitrogen) or cells in buffer RLT and purifying the RNA using QIAGEN RNA prep kit. Complimentary DNA was synthesized using QIAGEN omniscript RT kit. Real-time PCR was performed using the TaqMan system (Applied Biosystems; Foster City, CA) according to the manufacturer's protocol.

Statistics

All data were analyzed for statistical significance using the Student's t test. P values are as indicated.

Supplementary Text

Nanoparticle Characterization.

We have further characterized the iron oxide nanoparticles purchased from Ocean Nanotech (Catalog # SHP-20-50). The particles were coated with oleic acid and a proprietary polymeric coating, which is carboxy-terminated for further functionalization. The particles were specified to be 20 nm in diameter with a standard deviation of < 5%. This was confirmed in the current work; TEM analysis of the size distribution yielded an average diameter of 19.8 ± 2.7 nm (Fig. S2B). The particles were estimated to have a 4 nm oleic acid/polymeric coating in addition to the nanoparticle diameter observed in TEM. X-ray photoelectron spectroscopy (XPS) allowed identification of all elements within ~5 nm of the nanoparticle surface, as well as a more precise investigation of the nanoparticle surface chemistry and iron oxide content. XPS characterization (Fig. S2C) of the IONP indicated only the presence of iron, oxygen and carbon as would be expected from the polymeric coating. The shoulder in the C1s peak is consistent with the presence of carboxyl groups, as indicated in Fig. S2D. Moreover, the structure of the iron oxide particles was indicated by Ocean Nanotech to be magnetite (Fe_3O_4) for this particle size. However, magnetite and maghemite (γ-Fe_2O_3) is difficult to distinguish using x-ray diffraction (XRD) due to similarities in crystal structure. Indeed, comparison with JCPDS files #39-1346 (maghemite) and #75-0033 (magnetite) indicates that the current iron oxide particles are likely a mixture of both crystallographic structures.

We have also performed new studies to extend our analysis of the heating characteristics of the nanoparticles at different frequencies. A limited number of frequencies are suitable for medical use in addition to the 465 kHz used in our report so we also tested the heating of particles using a frequency of 13.56 Mhz which is the lowest of the remaining available frequencies and therefore the least likely to result in non-specific adsorption. The power level chosen was the maximum level that did not result in significant heating of water (200 W) in the absence of nanoparticles. At 465kHz, we observed a rapid increase in temperature for a suspension of 20nm iron oxide nanoparticles with a temperature increase of 17^{o}C that reached a plateau at 300s. A smaller rise in temperature (6^{o}C) was seen with 25nm particles with only minimal heating for larger sizes of iron oxide nanoparticle. In contrast, at 13.56MHz, there was significant heating for a broader range of particle sizes (10-25nm) with greatest heating observed for 15nm particles (11^{o}C) and very little heating of 20nm particles, with only a maximum temperature rise of 2^{o}C. However, the heating rate for 15nm particles was lower than that for 20nm particles at 465kHz and did not plateau over the test period. The heating of 25nm particles was similar at both frequencies.

Nanoparticle heating

Temperature decay from the iron oxide nanoparticle (IONP) surface has been explored extensively (*30*-*33*) and is complicated by factors such as the heat capacity of the surrounding medium, the nanoparticle ligand coating, and diffusion away from the nanoparticle surface. The change in temperature in the vicinity of the nanoparticle decreases as the inverse of the radius, and may be approximated by the conductive heat transfer equation (Fourier's Law)(*34*):

$$\Delta T = \frac{V_{np} Q}{4\pi k} \frac{1}{r} = \frac{q \rho D^2}{12k}$$

where V_{np} is the nanoparticle volume, Q is the total dissipated heat, r is the nanoparticle radius, q is the heating rate (W g^{-1}), ρ is the nanoparticle density, D is the diameter of the heated volume, and k is the thermal conductivity of water (0.64 W m^{-1} $^\circ$C^{-1}). Though it has been calculated that heating sufficient to trigger channel activation cannot be achieved on the single nanoparticle scale (ΔT ~ 10^{-5}°C/particle), it has been shown that accumulating a significant number of iron oxide nanoparticles in a small volume may raise the temperature sufficiently to have an effect. In a separate study, thermoresponsive polymer coatings on iron oxide nanoparticles have demonstrated increased drug release in radiofrequency fields, indicating that heating at the nanoparticle surface affected the structure of the thermopolymer and drug release profile. Both calculations and experiments in the literature have confirmed that ~1.2 mg of IONP are required to raise the temperature of a 1 cm^3 region by 5˚C (*35*). Based on this published literature and assuming a cell volume of 9.05 x 10^{-10}ml, we would require 1.1 x 10^{-9} mg/cell (ie 1.1pg/cell) to give a nanoparticle density of 1.2mg/ml to cause a local 5^{o}C increase in temperature. From EM images, we observe an average of 2 x 10^5 nanoparticles/cm. Assuming the particles are evenly distributed, this would give 4 x 10^{10} nanoparticles/cm^2. For a 20 µm cell, the surface area is 1.25 x 10^{-5} cm^2 (assuming a sphere) and therefore the calculated number of nanoparticles decorating the cell is 5 x 10^5 nanoparticles. The density of Fe_3O_4 is 5.24 g/cm3, and each nanoparticle is 20 nm in diameter, giving a nanoparticle weight of 1.75x10^{-16}g. Therefore, to achieve 1.1

picograms of nanoparticles per cell we would need at least 6.26 x 10^3 nanoparticles. We calculate that we have almost 100 fold greater nanoparticle decoration than that required to achieve a 5^{o}C local increase in temperature.

Transfecting cells with the ferritin construct resulted in the distribution of nanoparticles throughout the cell cytoplasm and with an average distance of the ferritin nanoparticle to the TRPV ion channel approximately equal to the cell radius. Previous mathematical modeling predicts that particles within 200nm would lead to sufficient heating to trigger channel activation *(19)*. We therefore quantified the number of ferritin nanoparticles within 200 nm of the cell membrane by EM. We found that there are 12.6 ± 2.86 particles per 0.2 μm^2 with an average distance to the cell membrane of 60.3 ± 2.85 nm. This distance is not dissimilar from the average distance between nanoparticles bound to transmembrane biotin acceptor protein tether (100 nm). Assuming the ferritin particles are evenly distributed through the cell, this would give 5 x 10^8 ferritin particles/cm^3. This is in considerable excess of the 1.1pg of iron (5 x 10^5 nanoparticles assuming ferritin has a similar composition to iron oxide nanoparticles but 10nm diameter) calculated to be necessary to achieve a 5^{o}C increase in temperature.

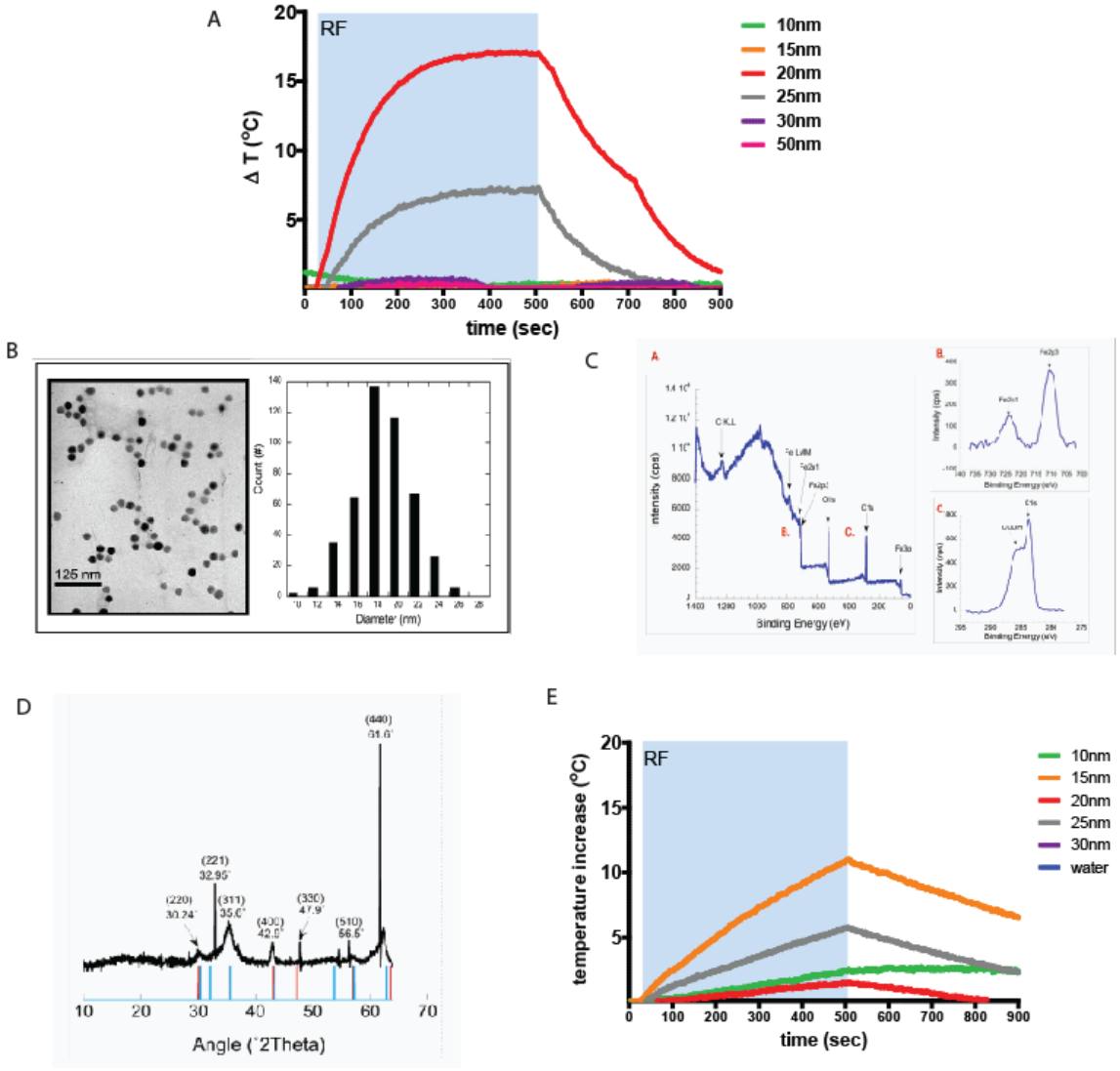

Figure S1: Heating of iron oxide nanoparticles in RF magnetic field

A) Bulk heating effects of treating iron oxide nanoparticle suspensions (1 mg/ml, 10-50 nm) in water with 465 kHz RF magnetic field. B) TEM of Ocean Nanotech (SHP-20-50) iron oxide nanoparticles and their size distribution, calculated to be 19.83±2.7 from 450 particles. C) X-ray photoelectron spectroscopy of iron oxide nanoparticle samples. Survey indicated the presence of iron, carbon and oxygen with iron content investigated in upper inset and the presence of carboxyl groups confirmed in the lower inset. D) XRD pattern of iron oxide nanoparticles compared with JCPDS patterns #39-1346 (γ-Fe_2O_3) and #75-0033(Fe_3O_4). E) Bulk heating effects of treating iron oxide nanoparticle suspensions (1 mg/ml, 10-30 nm) in water with 13.56Mhz, 200W, RF magnetic field.

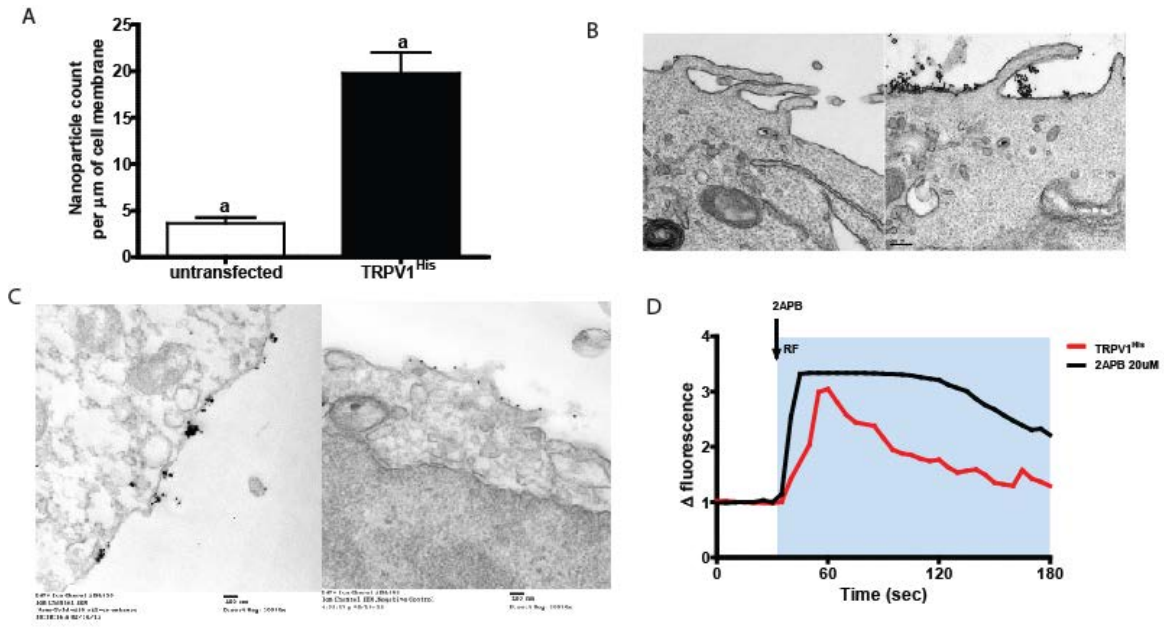

Figure S2: Nanoparticle decoration of cells in vitro

A) Nanoparticle decoration of cells *in vitro*. Significant nanoparticle binding to the surface of HEK293T cells expressing His tagged TRPV1 compared to untransfected cells. B) Electron micrograph of anti-His antibody coated iron oxide nanoparticles (20nm) binding to untransfected HEK293T cells (left panel) and HEK293T cells transfected with $TRPV1^{His}$ (right panel). Scale bar 200nm. C) Immunoelectron micrography of anti-His antibody coated iron oxide nanoparticles (20nm) co-localized with silver enhanced gold immunostaining for TRPV1 (10nm particles) in transfected HEK 293T cells (left panel). There is no TRPV1 immunostaining in the absence of the primary antibody (right panel). Scale bar as indicated. D) Representative changes in Fluo-4 fluorescence after application of TRP agonist 2APB or RF treatment in HEK 293T cells transfected with $TRPV1^{His}$ and decorated with nanoparticles.

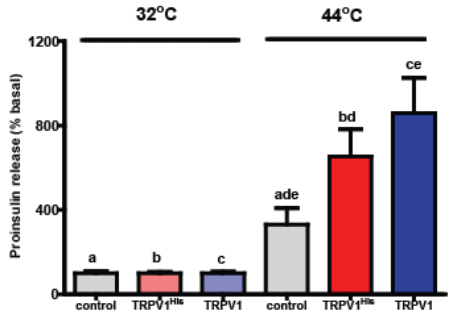

Figure S3: Temperature dependent release of proinsulin

Proinsulin release from HEK 293T cells transfected with calcium dependent insulin alone, $TPRV1^{His}$ and calcium dependent insulin or TRPV1 and calcium dependent insulin was examined at 32°C, below the threshold for TRPV1 activation and at 44°C, above the threshold for TRPV1 activation. Expression of $TRPV1^{His}$ and TRPV1 significantly increased proinsulin release at 44°C compared to that from cells without TRPV1. There is no significant difference in the proinsulin release seen with $TRPV1^{His}$ compared to unmodified TRPV1. (Same letter indicates $p < 0.05$).

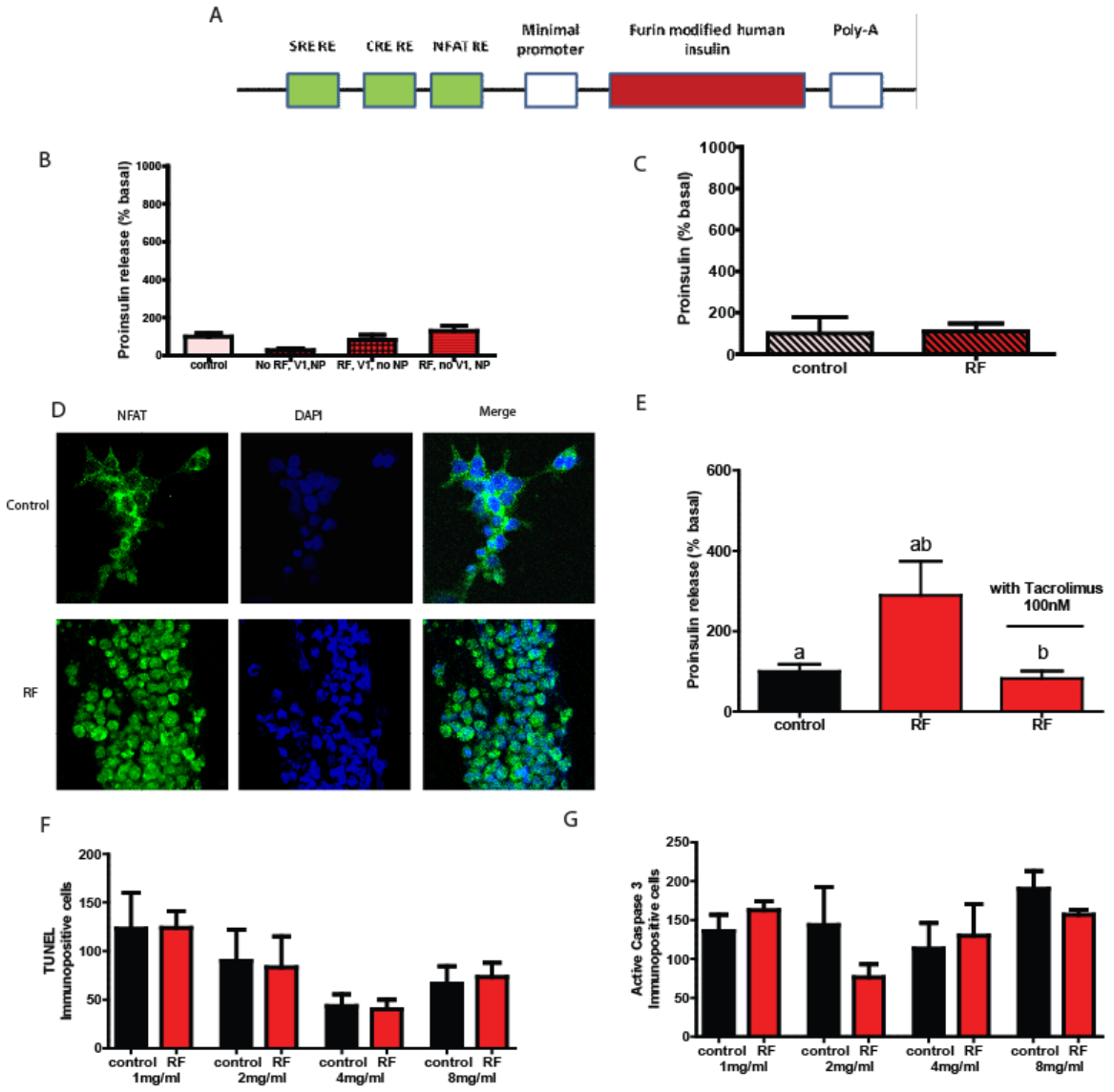

Figure S4: In vitro control studies

A) Bioengineered human insulin construct. Calcium dependent insulin release is via three calcium response elements: serum response element (SRE), cyclic AMP response element (CRE) and nuclear factor of activated T-cell response element (NFAT RE) and a minimal promoter upstream of a furin sensitive human insulin cDNA. B) RF treatment does not change proinsulin release from cells expressing the calcium dependent insulin gene from cells with TRPV1^{His}, calcium dependent human insulin and nanoparticles in the absence of RF treatment, from cells expressing TRPV1 and calcium dependent human insulin treated with RF but in the absence of nanoparticles, or from cells treated with RF expressing calcium dependent human insulin and binding nanoparticles via a nanoparticle tether comprised of a platelet derived growth factor receptor transmembrane domain with fused extracellular biotin acceptor protein but in the absence of TRPV1. C) The effects of nanoparticle heating are cell specific. Cells transfected with a nanoparticle tether, BAPTM, and mixed with cells transfected with TRPV1 and calcium dependent human insulin show no increase in proinsulin release with RF treatment. D) Translocation of NFAT1 with RF treatment. HEK 293T cells transfected with TRPV1^{His}/calcium dependent human insulin incubated with anti-His iron oxide nanoparticles show almost exclusively cytoplasmic NFAT immunostaining without RF treatment (control, upper panels). RF treatment results in NFAT staining in both the cytoplasm and nucleus of the cells (RF, lower panels).E) Effect of calcineurin inhibitor on RF dependent proinsulin release. Proinsulin release from RF treated HEK 293T cells transfected with TRPV1^{His}/calcium dependent human insulin incubated with anti-His iron

oxide nanoparticles was blocked by preincubation with Tacrolimus (100 nM). There is no difference apoptotic cells incubated with increasing concentrations of nanoparticles as assessed by TUNEL count (F) or activated Caspase-3 count (G) between untreated and RF treated cells transfected with $TRPV1^{His}$.

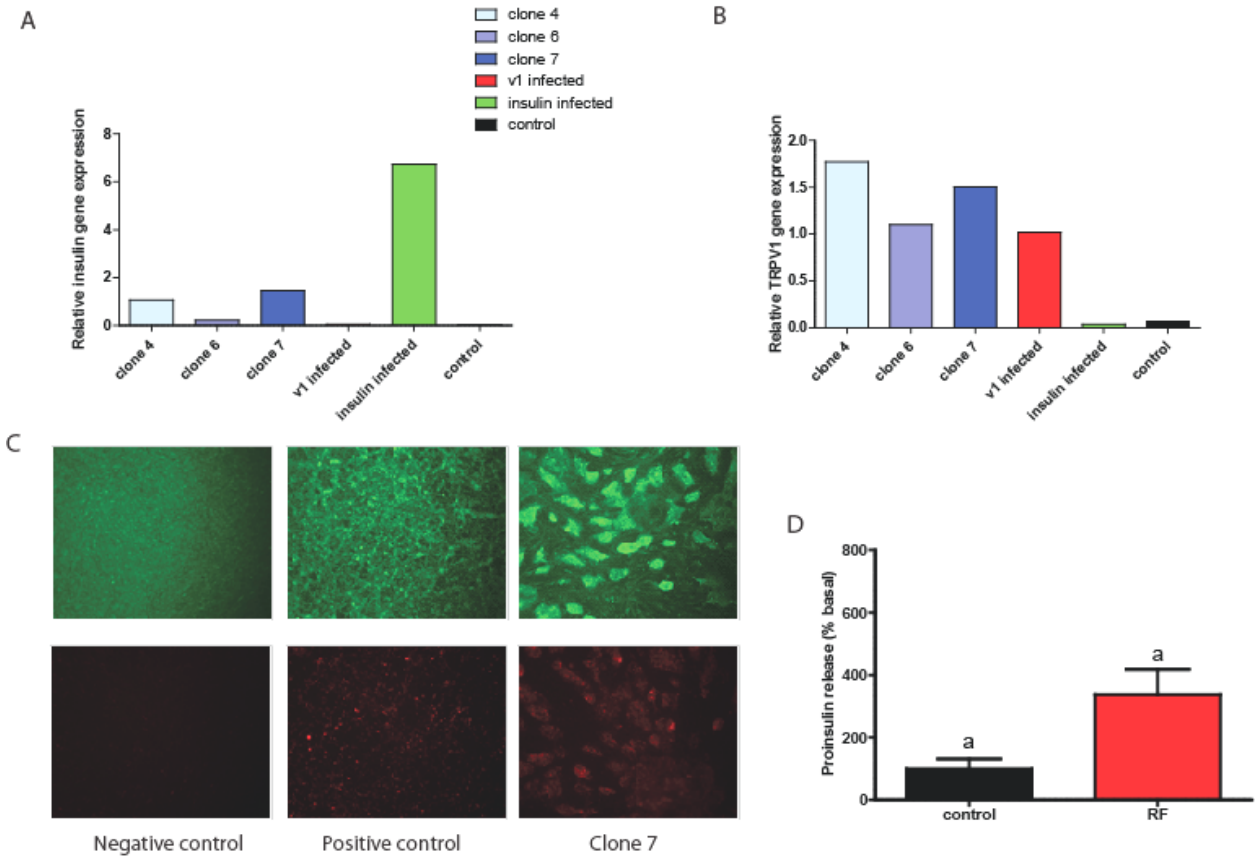

Figure S5: Expression of constructs and RF dependent proinsulin release from ES cells

A) Expression of insulin in ES cell clones: Quantitative PCR measured expression of human insulin in 3 ES cell clones (4, 6 and 7) electroporated with $TRPV1^{His}$ and Ca^{2+}-dependent human insulin construct along with cells stably expressing TRPV1 alone, Ca^{2+}-dependent human insulin construct alone or wild-type ES cells. B) Expression of TRPV1 in ES cell clones: Quantitative PCR measured expression of TRPV1 in 3 ES cell clones (4, 6 and 7) electroporated with $TRPV1^{His}$ and Ca^{2+}-dependent human insulin construct along with cells stably expressing TRPV1 alone, Ca^{2+}-dependent human insulin construct alone or wild-type ES cells. C) Immunohistochemistry for TRPV1 (upper panels) or His (lower panels) in wild-type cells (left panels), cells stably expressing $TRPV1^{His}$ (middle panels) or ES clone 7 (right panels). D) RF dependent proinsulin release from ES cells. ES clone 7 expressing TRPV1His and Ca^{2+}-dependent human insulin incubated with iron oxide nanoparticles show a significant increase in proinsulin release in response to RF treatment (same letter indicates $p < 0.05$).

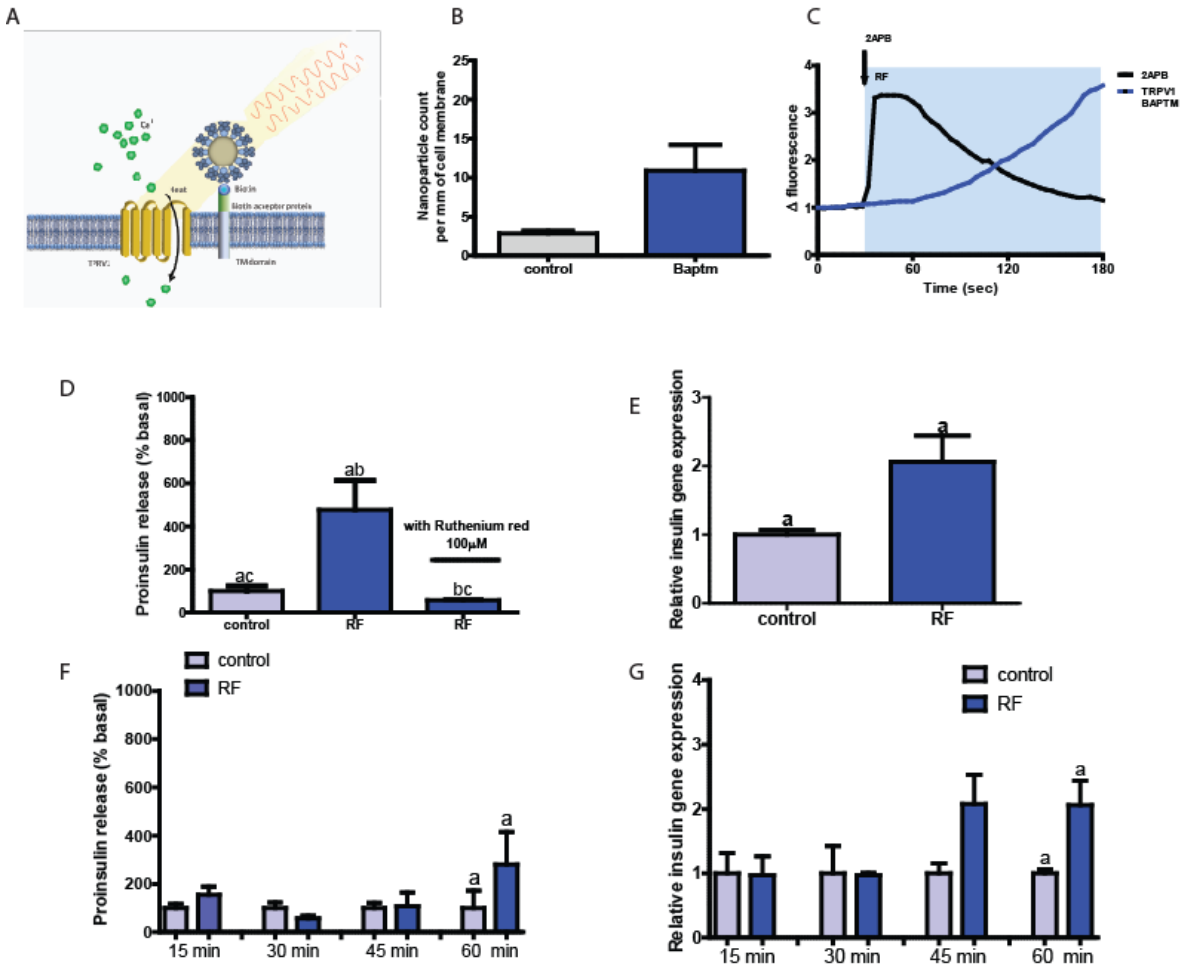

Figure S6: Dual component system for cell activation

A) Schema of dual component system. Streptavidin coated iron oxide nanoparticles bind biotin on a cell surface biotin acceptor protein fused to a transmembrane domain (BAPTM). Exposure to an RF field induces local heating, which opens TRPV1 channels. Calcium entry triggers downstream processes as before. B) Nanoparticle binding to the surface of HEK 293T cells expressing TRPV1 and BAPTM is increased compared to untransfected cells ($p = 0.09$). C) Representative changes in Fluo-4 fluorescence after application of TRP agonist 2APB or RF treatment in nanoparticle decorated HEK 293T cells transfected with dual component system. D) RF treatment increases proinsulin release *in vitro* from HEK 293T cells transfected with TRPV1, BAPTM and calcium dependent human insulin. This is blocked by Ruthenium red. (Same letter indicates $p < 0.05$). E) RF treatment increases insulin gene expression *in vitro* in cells with TRPV1, BAPTM and calcium dependent human insulin and is blocked by Ruthenium red. F) Time course of proinsulin release with RF treatment from HEK293T cells transfected with TRPV1, BAPTM and calcium dependent human insulin. G) Time course of insulin gene expression with RF treatment in cells transfected with TRPV1, BAPTM and calcium dependent human insulin.

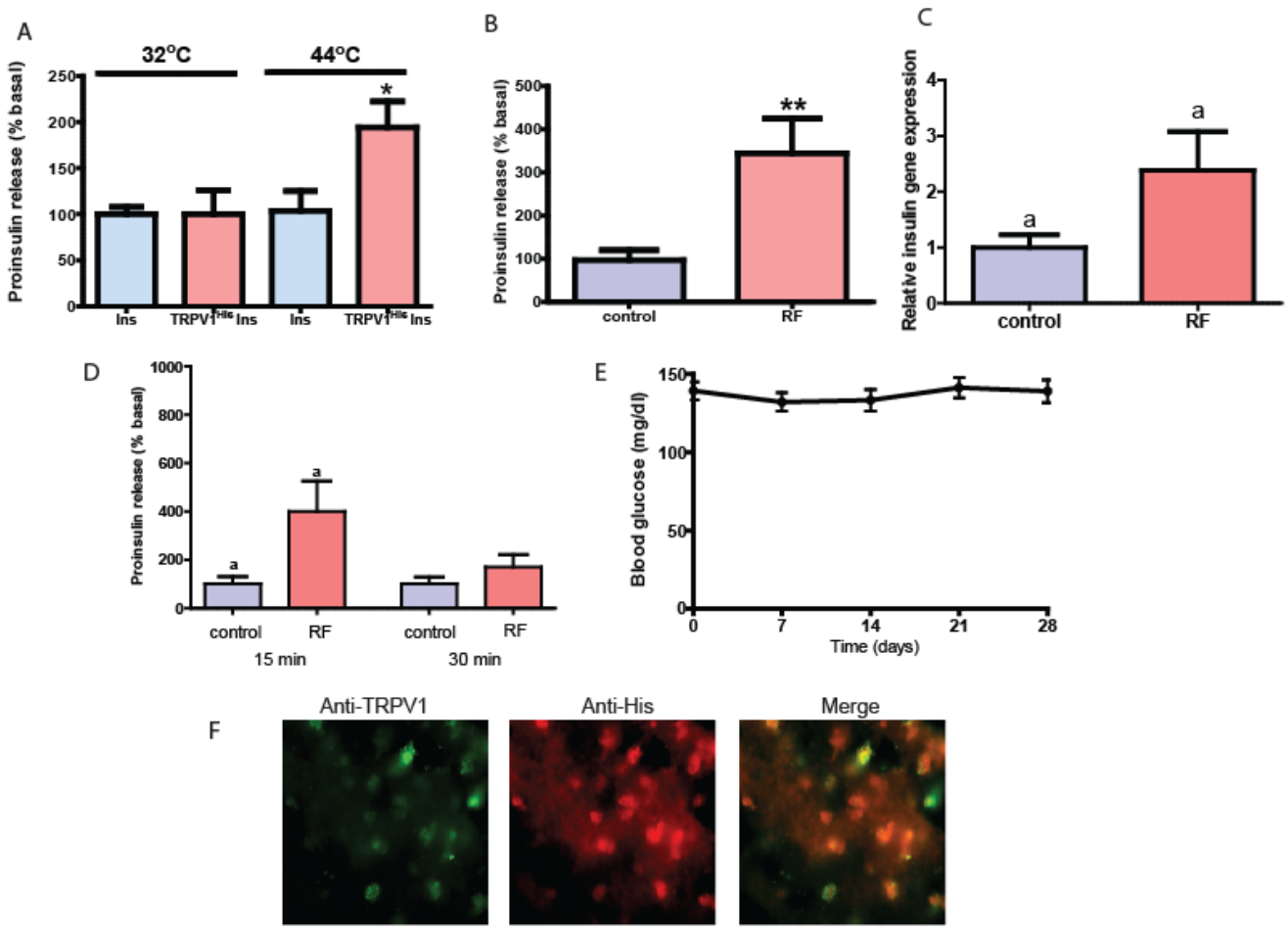

Figure S7: In vitro and in vivo studies on PC12 TRPV1^{His}/insulin stable cell line

A) Proinsulin release from PC12 cells stably expressing TRPV1^{His} and calcium dependent human insulin was significantly increased by a temperature above the threshold for TRPV1 activation (Same letter indicates $p < 0.05$) . B) RF treatment significantly increased proinsulin release from PC12 cells stably expressing TRPV1^{His} and calcium dependent human insulin. Same letter indicates $p < 0.01$). C) RF treatment significantly increases insulin gene expression in PC12 cells stably expressing TRPV1^{His} and calcium dependent human insulin. (Same letter indicates $p < 0.05$). D) Time course of proinsulin release from PC12 cells stably expressing TRPV1His and calcium dependent human insulin. RF treatment for 15 minutes significantly increased proinsulin release. E) Serial blood glucose measurement in nude mice injected with PC12 cells expressing TRPV1^{His} and calcium dependent human insulin to form a subcutaneous tumor. F) Immunohistochemistry for TRPV1 and His epitope tag in sections from tumors formed following subcutaneous injection of PC12 cells stably expressing TRPV1^{His} and calcium dependent human insulin.

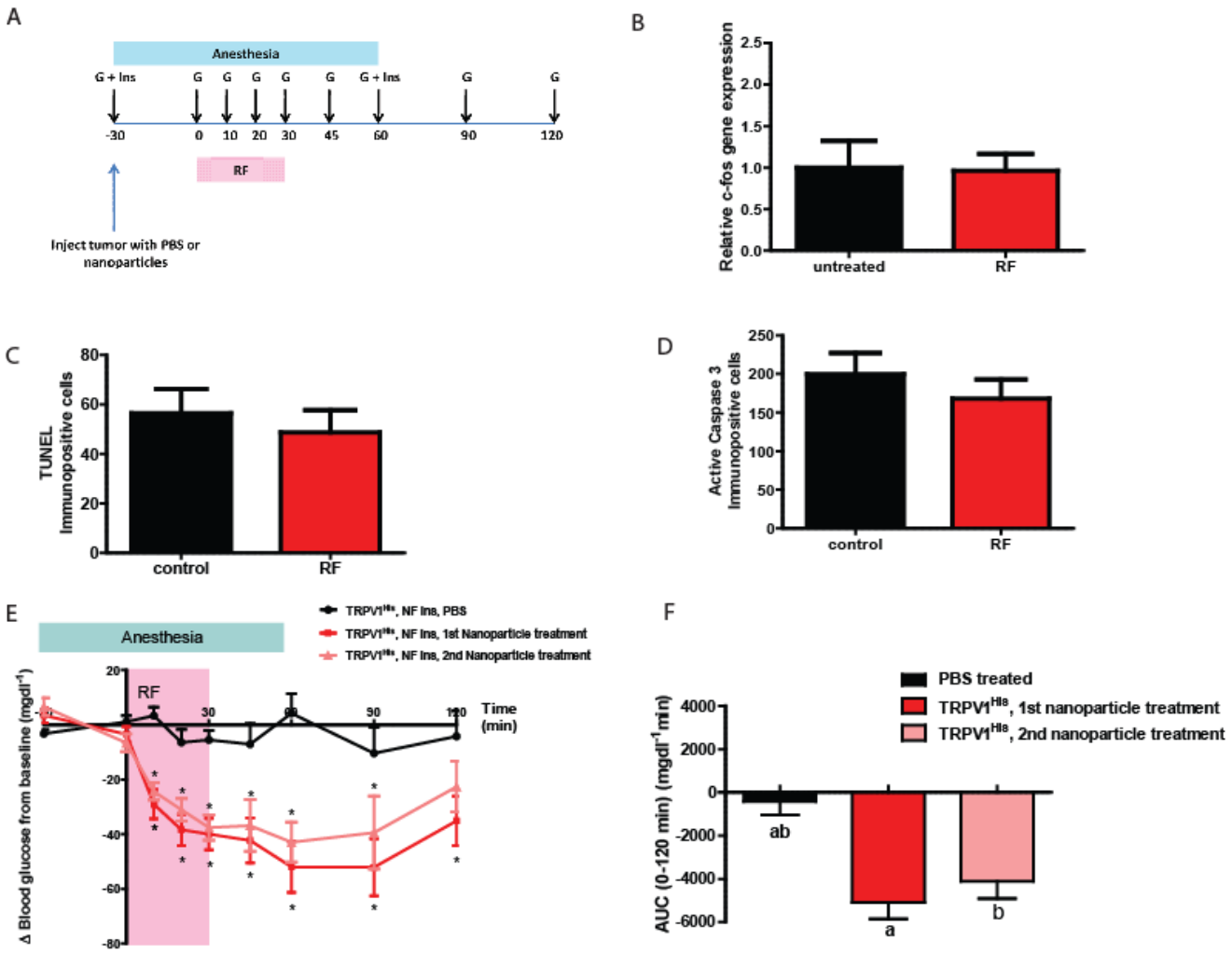

Figure S8:Nanoparticle regulation of blood glucose *in vivo*

A) Protocol for assessment of effects of RF treatment on blood glucose in mice bearing tumors expressing $TRPV1^{His}$ and calcium dependent human insulin. At time -30 min, mice are anesthetized and injected with PBS or nanoparticles. RF stimulation begins at time 0 and continues for 30 mins. Mice remain anesthetized for a further 30 mins. Samples for plasma insulin are taken at -30 and +30 mins and samples for blood glucose are taken before, during and after RF stimulation. B) Expression of c-fos gene in tumors showed no difference in levels between control (untreated) and RF treated tumors. C) No increase in apoptotic cells from nanoparticle and RF treated tumors as assessed by TUNEL. D) No increase in apoptotic cells from nanoparticle and RF treated tumors as assessed by IHC for activated Caspase-3. E) Effects of RF treatment on blood glucose in PBS and nanoparticle treated mice with tumors expressing $TRPV1^{His}$ and calcium dependent human insulin. RF treatment significant reduces blood glucose in nanoparticle treated mice compared to PBS treated mice in both the first and second study separated by a week. (Asterisk indicates $p < 0.05$.) F) Cumulative blood glucose change, measured by area under the curve, shows a significant decrease in nanoparticle treated mice compared to PBS treated mice in both the first and second study. There is no significant difference between the AUC for the nanoparticle studies.

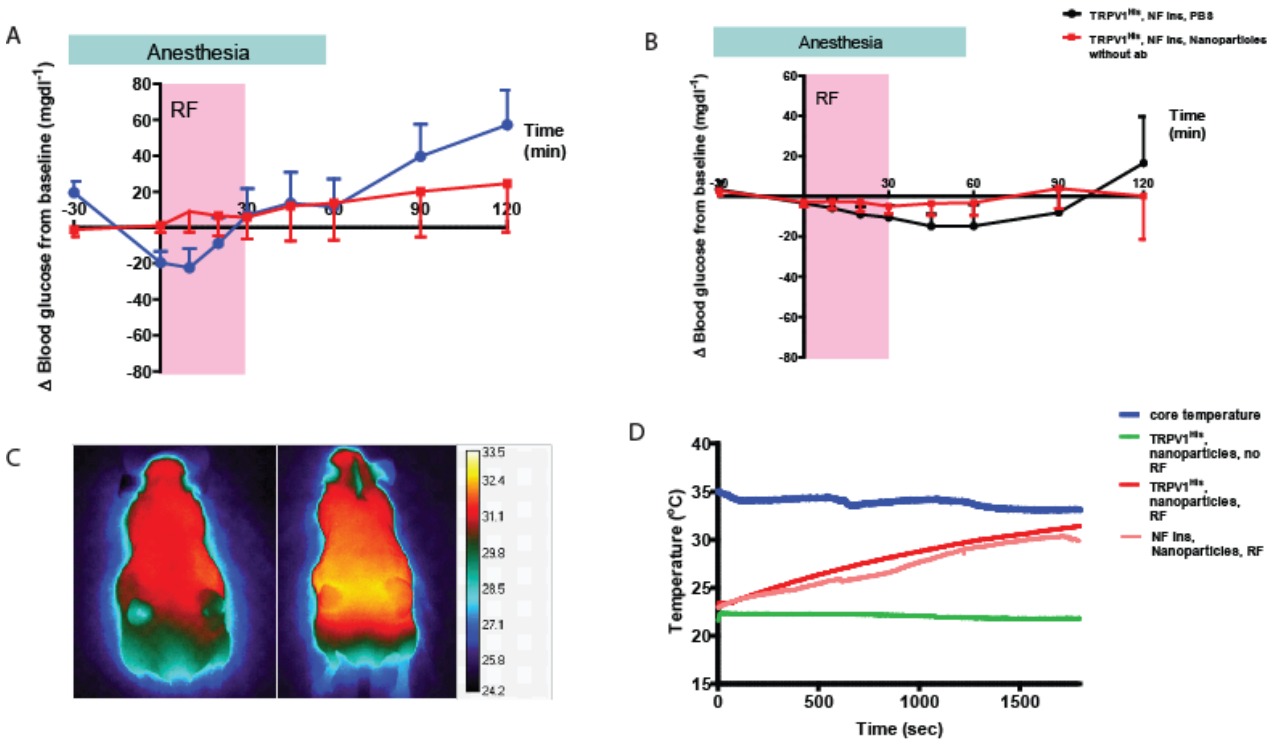

Figure S9: Effect of NICE in the absence of TRPV1, absence of anti-His antibodies and temperature studies *in vivo*

A) Effect of RF stimulation on blood glucose in PBS and nanoparticle treated mice bearing tumors expressing calcium dependent insulin gene without TRPV1. B) Effect of RF stimulation on blood glucose in mice treated with PBS or nanoparticles which have not been conjugated to anti-His antibody. C) Thermal imaging using an infrared camera on mouse with tumor expressing $TRPV1^{His}$ and calcium dependent human insulin injected with iron oxide nanoparticles before (left panel) and after (right panel) RF magnetic field treatment. C) Core body temperature and intra-tumor temperature recordings from mice with $TRPV1^{His}$ expressing tumors following nanoparticle injection with and without RF treatment and in mice with tumors without TRPV1 with nanoparticle injection and RF treatment. There is no difference in the intratumoral temperature achieved with RF treatment in the tumors of mice with $TRPV1^{His}$ and insulin expression compared to the tumors of mice with insulin expression but without $TRPV1^{His}$ expression.

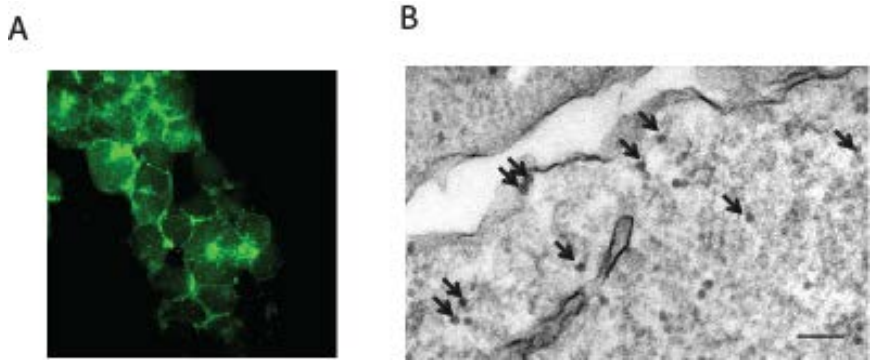

Figure S10: Expression of Ferritin fusion protein *in vitro*

A) Ferritin expression as shown by IHC for ferritin light chain. B) Electron micrograph of iron loaded ferritin in transfected cells. Scale bar 200nm.

References and Notes

1. E. Gellhorn, R. Cortell, J. Feldman, The autonomic basis of emotion. *Science* **92**, 288 (1940). doi:10.1126/science.92.2387.288 Medline

2. G. Stock, V. Sturm, H. P. Schmitt, K. H. Schlör, The influence of chronic deep brain stimulation on excitability and morphology of the stimulated tissue. *Acta Neurochir. (Wien)* **47**, 123 (1979). doi:10.1007/BF01404668 Medline

3. C. C. McIntyre, W. M. Grill, Extracellular stimulation of central neurons: Influence of stimulus waveform and frequency on neuronal output. *J. Neurophysiol.* **88**, 1592 (2002). Medline

4. E. S. Boyden, F. Zhang, E. Bamberg, G. Nagel, K. Deisseroth, Millisecond-timescale, genetically targeted optical control of neural activity. *Nat. Neurosci.* **8**, 1263 (2005). doi:10.1038/nn1525 Medline

5. J. H. Young, M. T. Wang, I. Brezovich, Frequency/depth-penetration considerations in hyperthermia by magnetically induced currents. *Electron. Lett.* **16**, 358 (1980). doi:10.1049/el:19800255

6. P. R. Strauffer, T. C. Cetas, R. C. Jones, Magnetic induction heating of ferromagnetic implants for inducing localized hyperthermia in deep-seated tumors. *IEEE Trans. Biomed. Eng.* **31**, 235 (1984). doi:10.1109/TBME.1984.325334 Medline

7. H. H. Richardson *et al*., Thermooptical properties of gold nanoparticles embedded in ice: Characterization of heat generation and melting. *Nano Lett.* **6**, 783 (2006). doi:10.1021/nl060105l Medline

8. K. Hamad-Schifferli, J. J. Schwartz, A. T. Santos, S. Zhang, J. M. Jacobson, Remote electronic control of DNA hybridization through inductive coupling to an attached metal nanocrystal antenna. *Nature* **415**, 152 (2002). doi:10.1038/415152a Medline

9. J. P. Fortin *et al*., Size-sorted anionic iron oxide nanomagnets as colloidal mediators for magnetic hyperthermia. *J. Am. Chem. Soc.* **129**, 2628 (2007). doi:10.1021/ja067457e Medline

10. B. Samanta *et al*., Protein-passivated Fe(3)O(4) nanoparticles: Low toxicity and rapid heating for thermal therapy. *J. Mater. Chem.* **18**, 1204 (2008). doi:10.1039/b718745a Medline

11. A. Z. Wang *et al*., Biofunctionalized targeted nanoparticles for therapeutic applications. *Expert Opin. Biol. Ther.* **8**, 1063 (2008). doi:10.1517/14712598.8.8.1063 Medline

12. J. DeFalco *et al*., Virus-assisted mapping of neural inputs to a feeding center in the hypothalamus. *Science* **291**, 2608 (2001). doi:10.1126/science.1056602 Medline

13. R. G. Thorne, C. Nicholson, In vivo diffusion analysis with quantum dots and dextrans predicts the width of brain extracellular space. *Proc. Natl. Acad. Sci. U.S.A.* **103**, 5567 (2006). doi:10.1073/pnas.0509425103 Medline

14. G. E. Hardingham, H. Bading, Calcium as a versatile second messenger in the control of gene expression. *Microsc. Res. Tech.* **46**, 348 (1999). doi:10.1002/(SICI)1097-0029(19990915)46:6<348::AID-JEMT3>3.0.CO;2-A Medline

15. A. Rao, Signaling to gene expression: Calcium, calcineurin and NFAT. *Nat. Immunol.* **10**, 3 (2009). doi:10.1038/ni0109-3 Medline

16. A. L. Shifrin, A. Auricchio, Q. C. Yu, J. Wilson, S. E. Raper, Adenoviral vector-mediated insulin gene transfer in the mouse pancreas corrects streptozotocin-induced hyperglycemia. *Gene Ther.* **8**, 1480 (2001). doi:10.1038/sj.gt.3301544 Medline

17. M. Tewari *et al*., Yama/CPP32 beta, a mammalian homolog of CED-3, is a CrmA-inhibitable protease that cleaves the death substrate poly(ADP-ribose) polymerase. *Cell* **81**, 801 (1995). doi:10.1016/0092-8674(95)90541-3 Medline

18. Y. Gavrieli, Y. Sherman, S. A. Ben-Sasson, Identification of programmed cell death in situ via specific labeling of nuclear DNA fragmentation. *J. Cell Biol.* **119**, 493 (1992). doi:10.1083/jcb.119.3.493 Medline

19. H. Huang, S. Delikanli, H. Zeng, D. M. Ferkey, A. Pralle, Remote control of ion channels and neurons through magnetic-field heating of nanoparticles. *Nat. Nanotechnol.* **5**, 602 (2010). doi:10.1038/nnano.2010.125 Medline

20. J. L. Farrant, An electron microscopic study of ferritin. *Biochim. Biophys. Acta* **13**, 569 (1954). doi:10.1016/0006-3002(54)90376-5 Medline

21. B. Sana, E. Johnson, K. Sheah, C. L. Poh, S. Lim, Iron-based ferritin nanocore as a contrast agent. *Biointerphases* **5**, FA48 (2010). doi:10.1116/1.3483216 Medline

22. K. Ziv *et al*., Ferritin as a reporter gene for MRI: Chronic liver over expression of H-ferritin during dietary iron supplementation and aging. *NMR Biomed.* **23**, 523 (2010). doi:10.1002/nbm.1491 Medline

23. B. Iordanova, C. S. Robison, E. T. Ahrens, Design and characterization of a chimeric ferritin with enhanced iron loading and transverse NMR relaxation rate. *J. Biol. Inorg. Chem.* **15**, 957 (2010). doi:10.1007/s00775-010-0657-7 Medline

24. D. Halperin *et al*., in *Proceedings of the 2008 IEEE Symposium on Security and Privacy*, Oakland, CA, 18 to 21 May 2008, pp. 129–142.

25. S. A. Hanna, paper presented at the Third International Symposium on Medical Information and Communication Technology, Montreal, Canada, 24 to 27 February 2009, .

26. A. C. Nathwani *et al*., Adenovirus-associated virus vector-mediated gene transfer in hemophilia B. *N. Engl. J. Med.* **365**, 2357 (2011). doi:10.1056/NEJMoa1108046 Medline

27. C. A. Butts *et al*., Directing noble metal ion chemistry within a designed ferritin protein. *Biochemistry* **47**, 12729 (2008). doi:10.1021/bi8016735 Medline

28. M. J. Caterina *et al*., The capsaicin receptor: A heat-activated ion channel in the pain pathway. *Nature* **389**, 816 (1997). doi:10.1038/39807 Medline

29. A. J. Giustini, R. Ivkov, P. Hoopes, Magnetic nanoparticle biodistribution following intratumoral administration. *Nanotechnology* **22**, 345101 (2011). doi:10.1088/0957-4484/22/34/345101 Medline

30. L. Rast, J. Harrison, Computational modeling of electromagnetically induced heating of magnetic nanoparticle materials for hyperthermic cancer treatment, Nanotech Conference and Expo 2010, Anaheim, CA, 21 to 24 June 2010, pp. 910–914.

31. R. Hergt *et al*., Physical limits of hyperthermia using magnetite fine particles. *IEEE Trans. Magn.* **34**, 3745 (2010). doi:10.1109/20.718537

32. O. Wilson, X. Hu, D. Cahill, P. Braun, Colloidal metal particles as probes of nanoscale thermal transport in fluids. *Phys. Rev. B* **66**, 224301 (2002). doi:10.1103/PhysRevB.66.224301

33. A. Jordan *et al*., Inductive heating of ferrimagnetic particles and magnetic fluids: Physical evaluation of their potential for hyperthermia. 1993. *Int. J. Hyperthermia* **25**, 499 (2009). doi:10.3109/02656730903287790 Medline

34. Y. Rabin, Is intracellular hyperthermia superior to extracellular hyperthermia in the thermal sense? *Int. J. Hyperthermia* **18**, 194 (2002). doi:10.1080/02656730110116713 Medline

35. A. Derfus *et al*., Remotely triggered release from magnetic nanoparticles. *Adv. Mater.* **19**, 3932 (2007). doi:10.1002/adma.200700091